Journal of the American Ceramic Society

RESEARCH ARTICLE

High Performance Phosphor-in-Glass Film on Grating Structure Sapphire Substrate for Laser Lighting

Mingchao Fang[1] | Wenting Ding[1] | Cihao Huang[1] | Baoping Zhang[1,2] | Yang Mei[1] | Leiying Ying[1] | Daquan Yu[1] | Rongbin Xu[1]

[1]School of Electronic Science and Engineering, Xiamen University, Xiamen, China | [2]Institute of Nanoscience and Applications, Southern University of Science and Technology, Shenzhen, China

Correspondence: Rongbin Xu (xurongbin@xmu.edu.cn)

Received: 27 March 2026 | **Revised:** 1 July 2026 | **Accepted:** 14 July 2026

Keywords: laser lighting | patterned sapphire substrate | phosphor-in-glass film | YAG:Ce

ABSTRACT

Laser lighting has the advantages of ultra-high brightness and luminous efficiency in the field of solid-state lighting. As one of the luminescence color converters for white laser lighting, phosphor-in-glass film (PiF) based on sapphire substrate is attracting much attention. In this work, a grating structure sapphire substrate (GS) with convex cross-section was fabricated. PiFs, consisting of melted silicon borate glass matrix and $Y_3Al_5O_{12}:Ce^{3+}$ phosphor powder, were prepared either on the same side (PiF-GS-S) or the opposite side (PiF-GS-O) of GS. Compared with PiF on planar sapphire (PiF-F), the incident blue laser beam is modulated by the pattern on the GS, which refracts the light and causes divergence of the laser beams. This expands the laser spot on the PiF, improving the uniformity of the laser beams. The saturation luminous flux of the PiF-GS-O under the 14.48 W/mm^2 laser excitation (1446 lm) is 49.7% higher and has a lower maximum temperature than those of the PiF-F, while maintaining a high luminous efficiency (150 lm/W). In addition, the effects of the two sintering methods on laser refracting are comparatively analyzed. The results demonstrate that the laser spot can be enlarged and homogenized by patterning the sapphire substrate, which finally helps to achieve higher luminous flux, higher luminous efficiency, and higher saturation threshold for laser lighting.

1 | Introduction

Solid-state lighting has evolved from incandescent lamps and fluorescent lamps to light-emitting diodes (LEDs) and laser diodes (LDs). Compared with LEDs, LDs have high power density, high brightness, and are free from the "efficiency droop" problem [1]. White LD lighting is achieved by irradiating blue laser beams onto a phosphor color converter. The yellow light is generated by the converter's absorption of the blue laser and mixes with the blue laser passing through the converter to produce white light [2]. Different from using organic epoxy or silica, phosphors need to be encapsulated in an extremely stable and high-temperature-resistant matrix to withstand the high-power-density laser from LDs [3, 4]. In recent years, several novel encapsulation forms of phosphor color converters have been studied, such as single crystals (SCs) [5, 6], transparent phosphor ceramics [7–9], composite phosphor ceramics [10–12], phosphor-in-glass bulk (PiG) [13, 14]. Because of the relatively low thermal conductivity of glass (~1 W·m^{-1}·K^{-1}), the laser resistance and luminescence performance of PiG are inferior to those of SC and TCP, a composite phosphor color converter was developed by sintering PiF on a high-thermal-conductivity substrate [14–22]. Among them, PiF also has advantages such as simple manufacturing process, low cost, and controllable luminescent properties [14–16].

In recent years, there has been growing interest in PiF on sapphire substrate, which has high thermal conductivity (~30W·m^{-1}·K^{-1})

and high transmittance (~85%) [17–19]. Many efforts such as using better binder materials and novel converter structure, have been made to further improve the luminescence performance of PiF [20, 21]. Lin et al. used full glass crystallization to improve the thermal conductivity of PiF, and measured a luminous flux (LF) of 632 lm at 12.5 W/mm^2 [23]. Wu et al. used colloidal silica instead of glass powder as an inorganic binder, which avoided the high-temperature sintering process. They measured an LF of 905 lm at a laser power of 3.72 W, and the saturation threshold reached 14.3 W/mm^2 [24]. However, when using new materials and processes, their impact on the phosphor crystals needs to be considered, and their ability to enhance the luminescence performance of converter is limited. Zhao et al. successfully fabricated a converter using a patterned sapphire substrate (PSS) with a conical moth-eye structure. At a laser power of 2.39 W, the device showed an LF of 577 lm [25]. Ding et al. fabricated a converter using a sapphire substrate with the similar pattern, and an LF of 721.2 lm at 6.29 W/mm^2 was measured [26]. However, the pattern affects the transmittance and light scattering when the laser incident from the substrate side. Low LF was obtained due to the incident blue laser was irradiated directly on the PiF in their works. It is worth noting that there has been no report on the fabrication of PiF on sapphire microlens array substrates and its laser illumination performance.

In this study, the grating structure sapphire substrate (GS) with convex cross-section was obtained through photolithography, photoresist thermal reflow, and inductively coupled plasma (ICP) etching methods [27, 28]. The fabricated substrates showed a high transmittance of ~80%. By sintering the YAG:Ce PiF on either the same side (PiF-GS-S) or opposite side (PiF-GS-O) of GS of these sapphire substrates, the luminescence performance of them showed obvious differences. As the laser power density increased to the saturation threshold, the LF of PiF-GS-S was close to that of PiF-F, while PiF-GS-O was nearly 50% higher than that of PiF-F, and a higher saturation threshold was obtained. Finally, the converging and diverging effects of the two converters on incident laser beams and emitted light spots were comparatively analyzed.

2 | Experiment

2.1 | Fabrication and Characterization of GS

Sapphire substrates were double-sides polished c-face (0001) SC with area of 7 × 7 mm^2 and thickness of 400 μm. A 20 μm-wide grating structure with convex cross-section was formed on the surface by using a standard photolithography and a thermal reflow process. The distance between two adjacent gratings was 10 μm. After the formation of the photoresist pillars, the sample was then placed onto a hotplate at 100°C for 10 min. The flat pillars melted and formed convex structures due to the surface tension. Then, an ICP etching process with Cl_2 and Ar as the etching gases was used to transfer the photoresist pattern to the surface of the sapphire substrate. The flow rates of Cl_2 and Ar were 40 and 15 sccm, respectively, and the source power and the bias power were 600 and 200 W, respectively.

After the GSs were fabricated, the patterns were investigated by an optical microscope and a step profiler. The transmittances of planar sapphire substrate (F) and GS were investigated using a UV-Vis spectrophotometer.

According to the results of microscope and step profiler, as shown in Figure 1a,b, the width and distance of GS meet the expectations, respectively were 20 and 10 μm. In the actual test, we used a blue laser to irradiate PiF. Thus, a single blue laser was irradiated on the F and GS to test their actual optical properties. The laser incident from flat side and pattern side are named as GS-F and GS-P, respectively. The corresponding spot photos of transmitted laser are shown in Figure 1c. Due to the high transmittance of the substrate, the laser spot does not show obvious deformation or divergence after transmission through the F, and still maintains the aggregated point-like spot. However, when the blue laser is irradiated on the GS, the transmitted light spot presents a linear, symmetrical, and evenly dispersed point pattern. It is worth noting that the transmitted laser spots were caused by the multiple-slit diffraction of different patterns. The transmittance of F was approximately 89% (Figure 1d). For GS, additional reflection loss was introduced after etching, and the transmittance of GS decreased. The transmittance of GS-P showed a slight increase compared to that of GS-F, being 79% and 82%, respectively. This can be attributed to the patterned structure can selectively reduce the reflection in the direction of incident light.

2.2 | Fabrication and Characterization of PiF

The fabrication process of PiFs through a solid-phase co-sintering method is illustrated in Figure 2a. First, a homogeneous mixture was prepared by combining commercial $Y_3Al_5O_{12}:Ce^{3+}$ (YAG:Ce) phosphor powder with $30SiO_2$-$22B_2O_3$-32ZnO-$10Na_2O$-6CaO (mol%) glass powder in a weight ratio of 3:1 using an agate mortar. In this work, the YAG:Ce phosphor powder used was purchased from Shenzhen looking long technology Co. Ltd., with an average particle diameter of 25 μm. The raw materials of the glass powder were from Shanghai Aladdin Co. Ltd. After mixing according to the ratio, it was melted at 1200°C for 1 h, then water quenched, dried, and ground thoroughly. Finally, the glass powder was obtained by filtering through a 200-mesh sieve. Then, an organic vehicle consisting of 97% terpineol and 3% ethyl cellulose (wt%) was added to the powder mixture at a weight ratio of 1:3 and thoroughly blended. After that, the resultant slurry was transferred to the surface of substrates and coated uniformly in a thickness of 60 μm with a blade. Following coating, the substrate was initially heated at 300°C for 6 h to burn out the organic, and followed by sintering at 700°C for 40 min in a muffle furnace. Finally, the samples were cooled gradually to room temperature. PiF could be sintered on different surfaces of substrates. As shown in Figure 2b, there were three structures of PiF converters: PiF-F was sintering the PiF directly on the flat substrate, and PiF-GS was sintered on either the same side of pattern or opposite side.

The photoluminescence excitation (PLE), photoluminescence (PL) emission spectra, fluorescence decay curves, and PL quantum yield (PLQY) of YAG:Ce phosphor and PiF were measured by a steady-state and transient fluorescence spectrometer with a 450 W Xenon lamp and a 450 nm laser excitation. The PiFs were irradiated by a 450 nm LD (10 W) with the laser spot area of 0.7 mm^2. The optical performances of PiFs, including LF, luminescence efficacy (LE), CCT, color-rendering index

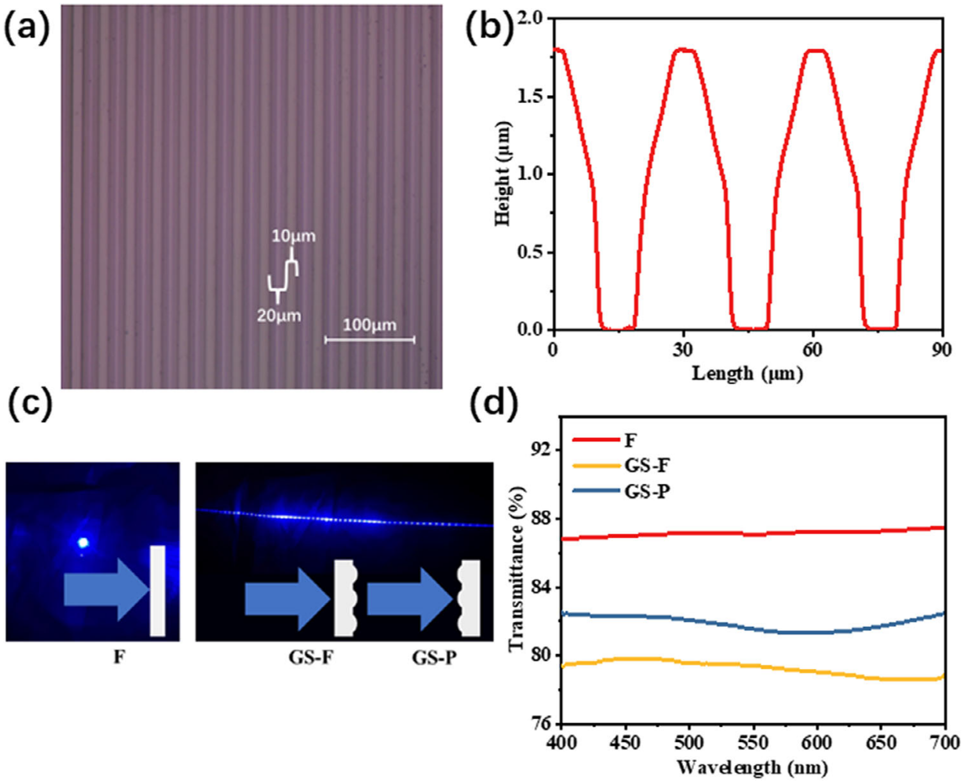

FIGURE 1 | (a) Optical image and (b) height of GS. (c) The picture of laser spot after passing through F and GS. (d) The transmittance of F, GS-F, and GS-P.

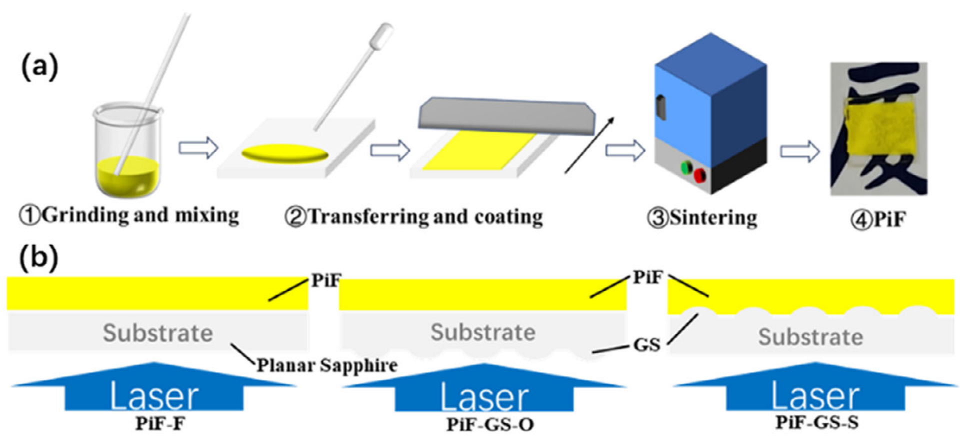

FIGURE 2 | (a) Schematic illustration of the fabrication process of the PiF. (b) Schematic diagram of the structures of the PiF-F, PiF-GS-O and PiF-GS-S.

(CRI), and electroluminescent (EL) spectra, were measured by a spectrometer detector with a 30 cm diameter integrating sphere.

Figure 3a–c shows the PLE and PL spectra, transient luminescent decay curves, and PLQY of YAG:Ce phosphor and PiF. Both the PLE spectra of YAG:Ce phosphor and PiF have two excitation peaks at ~345 and 455 nm, attributed to the electron transition of Ce^{3+} from 5d→4f energy level, and the PL spectra show the broadband emission (~560 nm) under 450 nm light excitation. Compared with those of original YAG:Ce phosphor, there were no obvious changes in spectral profile, lifetime or PLQY, confirming during the co-sintering process, the luminescence performance of YAG:Ce phosphor has well entertained. After that, the luminescence properties of PiFs were tested by the integrating sphere system.

3 | Result and Discussion

The luminescence performance of PiF-F, PiF-GS-S, and PiF-GS-O were investigated in the integrating sphere under the various laser power densities, as shown in Figure 4a–d. Initially,

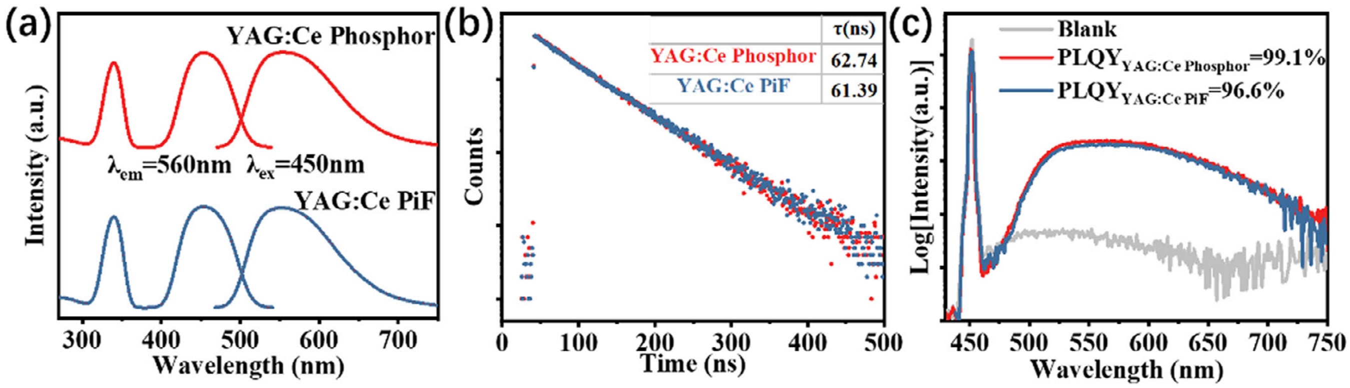

FIGURE 3 | (a) PLE and PL, (b) fluorescence decay curves and (c) PLQY of the YAG:Ce phosphor powder and PiF.

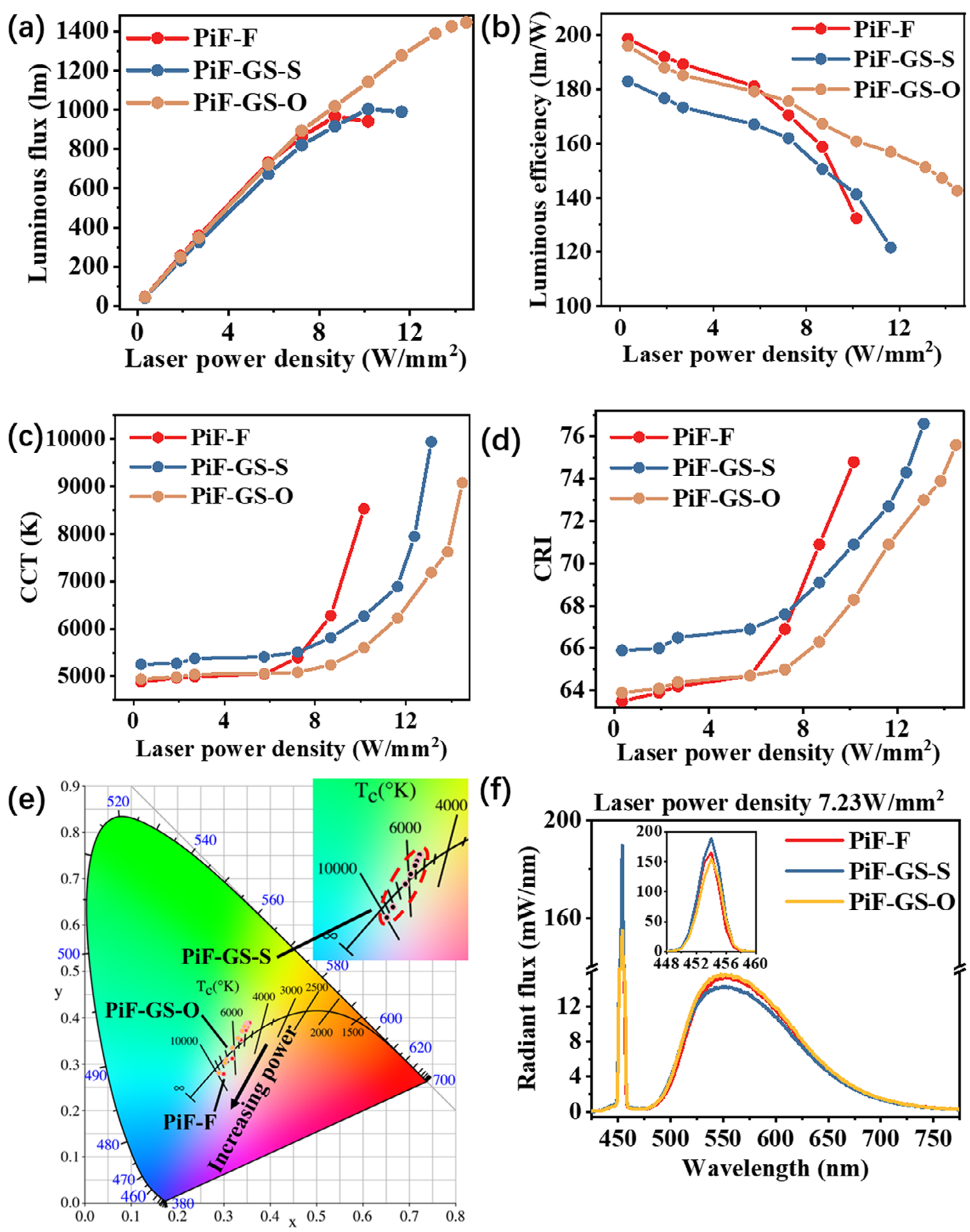

FIGURE 4 | (a) LF, (b) LE, (c) CCT, (d) CRI, and (e) CIE color coordinates of the samples at different laser power densities. (f) EL spectra of the samples at laser power density of 7.23 W/mm^2.

the LF of the samples increased monotonically with increasing incident LD power. But when the incident power density reached 8.69 W/mm^2, luminescence saturation was observed on PiF-F sample and then LF began to decline. The saturation threshold values of PiF-GS-S and PiF-GS-O, respectively were 10.15 and 14.48 W/mm^2. And the corresponding LF peak values for PiF-F, PiF-GS-S, and PiF-GS-O were 966.2, 1004, and 1446 lm, respectively. However, the LE of three samples decreases steadily as the indecent laser power density increases (Figure 4b). The average LE for PiF-F and PiF-GS-O exceeded 185 lm/W, and the LE of PiF-GS-S was a little lower than others, about 170 lm/W. The lower LE of PiF-GS-S was attributed primarily to the reduced transmittance of the substrate, as shown in Figure 1d. After reaching the saturation threshold, the heat around the incident laser spot in the PiF converters more excitation light energy into phonons or thermal ionization, which in turn further increases the temperature. When the laser power density was higher than the threshold, the heat cannot be efficiently dissipated, and the luminescence saturation would occur and LE would drop. In Figure 4c, the CCT of PiF-GS-S (~5200 K) was higher at the beginning due to the lower transmittance of substrate, which reflected more blue light in the integrated sphere, and correspondingly the CRI of PiF-GS-S (~67) was higher than that of other samples. Meanwhile, due to the transmittance of PiF-GS-O was higher than that of PiF-GS-S and close to PiF-F, and the diverging effect of the pattern, the CCT and CRI of PiF-GS-O (~4900K and ~64) were similar to those of PiF-F at the beginning, due to the yellow broadband emission limitation of YAG:Ce. The CRI values ranged between 63 and 76 for all samples, as shown in Figure 4d. Figure 4e investigates the CIE color coordinates variation of the emitted light, shift from yellow-white region to blue-white one. Figure 4f shows the EL spectra of these samples under the same laser power density of 7.23 W/mm^2. PiF-GS-S exhibited relatively low absorption of the blue laser light, resulting in weaker emission intensity. The transmittance of PiF-F and PiF-GS-O was higher, leads to enhanced absorption of blue light and an increase in emission intensity.

Figure 5a shows an enlarged view of the single period GS profile measured by step profiler. A second-order polynomial fitting was performed on these measurement data and is represented by the red line. The fitting function is shown in Equation (1), where A is 0.18782, B is 0.26964, and C is −0.01136. The square of the correlation coefficient between the experimental data and the fitting data is approximately 98%, which means that the prepared GS has a focusing effect similar to that of a curved lens.

$$y = A + Bx + Cx^2 \tag{1}$$

According to geometric and optical theories, for a convex lens with a certain thickness placed in an air medium, its focal length is determined by the thickness, the radius of curvature, and the refractive index of material [29]:

$$\frac{1}{f} = (n-1)\left(\frac{1}{R_1} - \frac{1}{R_2} + d \times \frac{n-1}{n} \times \frac{1}{R_1 R_2}\right) \tag{2}$$

where f is focal length, n is refractive index, R_1 and R_2 are radius of curvature (R), d is the thickness of the lens. Here, a single period pattern can be regarded as a plano-convex lens because one side of it is flat and R_2 tends to infinity. In PiF-GS-S, PiF and the pattern are sintered on the same side. Therefore, when the incident parallel light beam irradiates into the PiF layer from the lens, the refractive index of PiF needs to be considered, and Equation (2) is transformed into:

$$f = \frac{R}{\left(\frac{n_S}{n_P} - 1\right)} \tag{3}$$

where n_S is the refractive index of sapphire (1.78) and n_P is the refractive index of PiF (1.46) at a wavelength of 450 nm light. In Equation (3), R is calculated based on the second-order derivative of the quadratic term of the surface.

$$R = \frac{\left[1 + \left(\frac{dy}{dx}\right)^2\right]^{\frac{3}{2}}}{\left|\frac{d^2y}{dx^2}\right|} \tag{4}$$

Equations (1) and (4) can be used to calculate that the average R of the pattern is approximately 48 μm. By using Equation (3), it is calculated that the focal length of PiF-GS-S in the PiF layer should be 219 μm. Since the actual thickness of the PiF layer is 60 μm, the incident laser is refracted again when it transmits from the PiF layer to the air, and the remaining length is shortened to (219 − 60)/1.46 ≈ 108.9 μm. Finally, the distance from the focal point in the air to the lens is 168.9 μm.

As for PiF-GS-O, the pattern can be regarded as a plano-convex lens with a thickness of 400 μm, which means that the focal point of PiF-GS-O is inside the substrate. The Equation (5) shows the internal focal length f_s of the plano-convex lens:

$$f_S = \frac{R}{n_S - 1} \cdot n_S \tag{5}$$

Substituting the obtained R and n_S into Equation (5), the internal focal length of the GS can be calculated to be 109.5 μm.

Figure 5b,c shows the finite element simulation results of the refraction of blue laser caused by patterns when incident from the substrate side onto PiF-GS-S and PiF-GS-O, respectively. During the simulation, it was assumed that the blue laser is absorbed by the randomly distributed phosphor particles in the PiF, and the light stop at the edges of the phosphor particles. In addition, due to the aperture size of pattern is much larger than the wavelength of blue laser and the close proximity between the PiF and the substrate, the diffraction effect of the GS was omitted. Therefore, the ray optics simulation results simply demonstrate the effect of a single period pattern on the incident laser and its focal length. For PiF-GS-S, as shown in Figure 5b, the simulation result illustrates that after the incident laser is refracted by the pattern, it converges in the PiF layer and in the air, and finally the focal point is at a distance of ~170 μm from the pattern, which is consistent with the result calculated using Equation (3). Compared with PiF-GS-S, before the incident laser reaches the PiF layer of PiF-GS-O, it is not only affected by the pattern refraction and converges, but also diverges. The focal point is inside the substrate located about 100 μm away from the pattern, as shown in Figure 5c. After that, the beam width when it reaches the PiF layer is about 65 μm, which is about 2.8 times larger than the original width (assuming

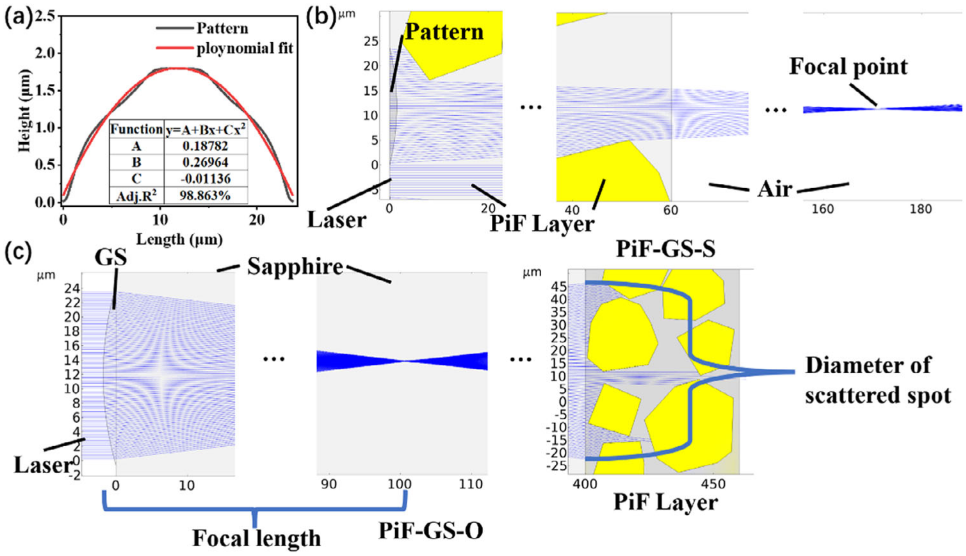

FIGURE 5 | (a) Cross-sectional surface profiles of single pattern and its profile fitting and function. Simplified structure of (b) PiF-GS-S and (c) PiF-GS-O and their refraction simulation of blue laser.

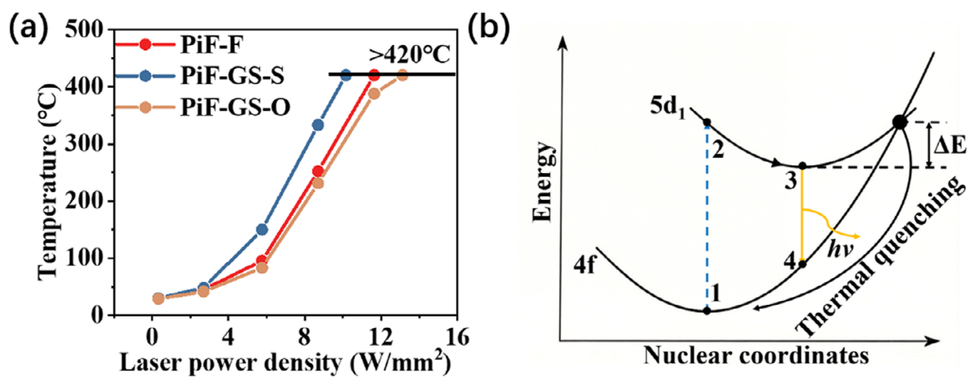

FIGURE 6 | (a) The maximum temperature varying with the incident laser power for PiF-F, PiF-GS-S, and PiF-GS-O after 30 s. (b) Configurational coordination diagrams illustrating the thermally quenching of Ce^{3+}.

the beam width before convergence is 23 µm). That is the reason why the PiF-GS-O get a higher LF, higher luminous efficiency, and higher saturation threshold than PiF-GS-S and PiF-F. In summary, the luminescence performance of PiF-F and PiF-GS is significantly affected by the pattern, especially the thickness of substrate is fully utilized in convergence and divergence when the laser is irradiated on the pattern.

To verify the thermal accumulation effect underlying luminescence saturation, the maximum surface temperatures of the three converters were measured using an IR thermography camera (the upper limit temperature is 420°C) after 30 s of continuous laser irradiation at various power densities, as shown in Figure 6a. The temperature of all three converters increases monotonically with increasing laser power density. However, the rate and magnitude of the temperature rise differ significantly among the three converters. PiF-GS-S exhibits the highest temperature at each power density. This is because the pattern on the incident side causes the laser beam to converge within the PiF layer, leading to a concentrated excitation spot and intense localized heating. PiF-F shows an intermediate temperature level, as the flat substrate provides neither additional focusing nor beam expansion. However, due to the substrate patterning increases the contact area between the PiF layer and the substrate of PiF-GS-S, which is helpful for heat conduction in a short time, PiF-GS-S does not show an obvious saturation threshold and an increase in LF compared with PiF-F (Figure 4a). Within a continuous excitation, the enhanced contact area between the PiF and the patterned substrate is insufficient to compensate for this effect. PiF-GS-O consistently exhibits the lowest temperature among the three configurations. In this converter, the laser is incident from the pattern side of the substrate, and then converges and diverges before it reaches the PiF layer, effectively reducing the local power density and alleviating heat accumulation. Consequently, PiF-GS-O maintains the lowest operating temperature and the highest saturation threshold.

The temperature rises rapidly after the saturation threshold, it can be explained by the model shown in Figure 6b. The Ce^{3+} in the phosphor absorbs the photon energy, the electrons transition

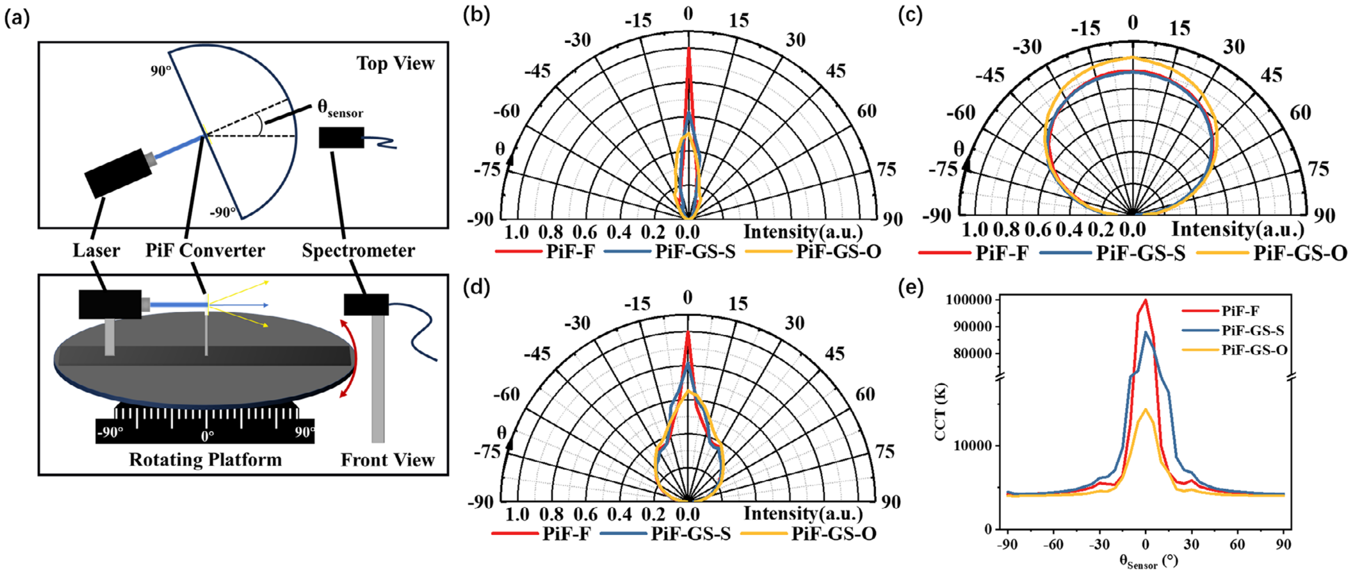

FIGURE 7 | (a) Schematic of the measurement setup for angular emission profile. Polar plots comparing the normalized intensities of the (b) transmitted blue light, (c) emitted light components, and (d) white light for PiF-F, PiF-GS-S, and PiF-GS-O. (e) Chart of angular CCT distribution for the converters.

from the 4f ground state to the $5d_1$ excited state. After lattice relaxation, electrons transition from the $5d_1$ back to the 4f ground state and emit photons. When the incident energy is large enough, the electrons in the $5d_1$ level energy relax to the intersection with the 4f energy level curve. After meeting the conditions for non-radiative cross-relaxation, the electrons return to the ground state in the form of vibrational relaxation. The intensity of the non-radiative cross-relaxation from $5d_1 \rightarrow 4f$ can be described by the non-radiative transition rate R_{nr} based on the Arrhenius equation, and the mathematical expression is as follows:

$$R_{nr} = A_{nr} \cdot \exp\left(-\frac{\Delta E}{k_0 T}\right) \tag{6}$$

where A_{nr} is the pre-factor of non-radiative recombination, k_0 is the Boltzmann constant, and T is the temperature. It can be seen from the equation that the higher the T, the larger the R_{nr}, which means that more Ce^{3+} changes from radiative transition to emit photons to non-radiative transition to emit phonons, thus reducing the luminous intensity of the phosphor and leading to thermal quenching.

In general, when the heat in the PiF layer cannot be dissipated by the substrate in time, the R_{nr} of Ce^{3+} in the phosphor will increase, resulting in an increase in heat generation. This, in turn, leads to a cycle of increased heat and thermal quenching. Therefore, when the incident laser power density exceeds the saturation threshold, the operating temperature of the converter will increase significantly, and the LF will decrease.

To further study the luminescence performance affected by the pattern, the angular emission profiles of luminous intensity and CCT for the transmitted blue light (peak wavelength ~450 nm) and emitted light (wavelength 480–750 nm) components of the converter were measured. A rotatable measurement device was constructed. The top and front views of the structure are shown in Figure 7a, with measurement angles ranging from −90° to 90°. Figure 7b,c demonstrates the normalized intensities of the transmitted blue and emitted light components for PiF-F, PiF-GS-S, and PiF-GS-O, respectively. It is evident that PiF-F exhibits the highest blue light intensity at 0° with the smallest divergence angle (less than 10° FWHM), and the blue light intensity of PiF-GS-S and PiF-GS-O is lower. In addition, the divergence angle of PiF-GS-O for blue light is largest, which is approximately 25° FWHM, due to the refraction effects of the pattern on the incident laser, resulting in more uniform distribution. The blue light intensity and divergence angle of PiF-GS-S fall between the other two, as the pattern and the PiF are sintered on the same side, limiting the full divergence of the incident laser. Regarding the luminous intensity measurement of emitted light in Figure 7c, the curves in the polar plot appear as circles and symmetrical about the vertical axis, with yellow light intensity gradually decreasing as the angle increases. The divergence angles of these converters are similar. The emitted light intensities of PiF-GS-S and PiF-F are similar, while PiF-GS-O exhibits overall higher emitted light intensity, demonstrating that the refraction of the incident laser by the pattern elongates the optical path length, thereby exciting more phosphor particles. Figure 7d,e shows the results of luminous intensity and CCT varying with angle. The luminous intensity and CCT near 0° are influenced by the intensity of the transmitted blue light component. The luminous intensities at 0° are enhanced due to the transmitted blue light, and further illustrating the refraction effects of the pattern on the transmitted laser. PiF-GS-S shows a reduced CCT, while PiF-GS-O has the lowest CCT. The highest luminous intensity and CCT are observed in the PiF-F sample, with its CCT exceeding the instrument's measurement range (100 000 K). The luminous intensity of PiF-GS-O is relatively uniform, with the curve resembling an ellipse, and the distribution angle of PiF-GS-O is 70° FWHM, whereas the angles of PiF-F and PiF-GS-S are 20° and 30° FWHM, respectively. The CCTs of all three samples converge when θ increases, indicating that the emitted light in this range is predominantly yellow light from the PiF layer.

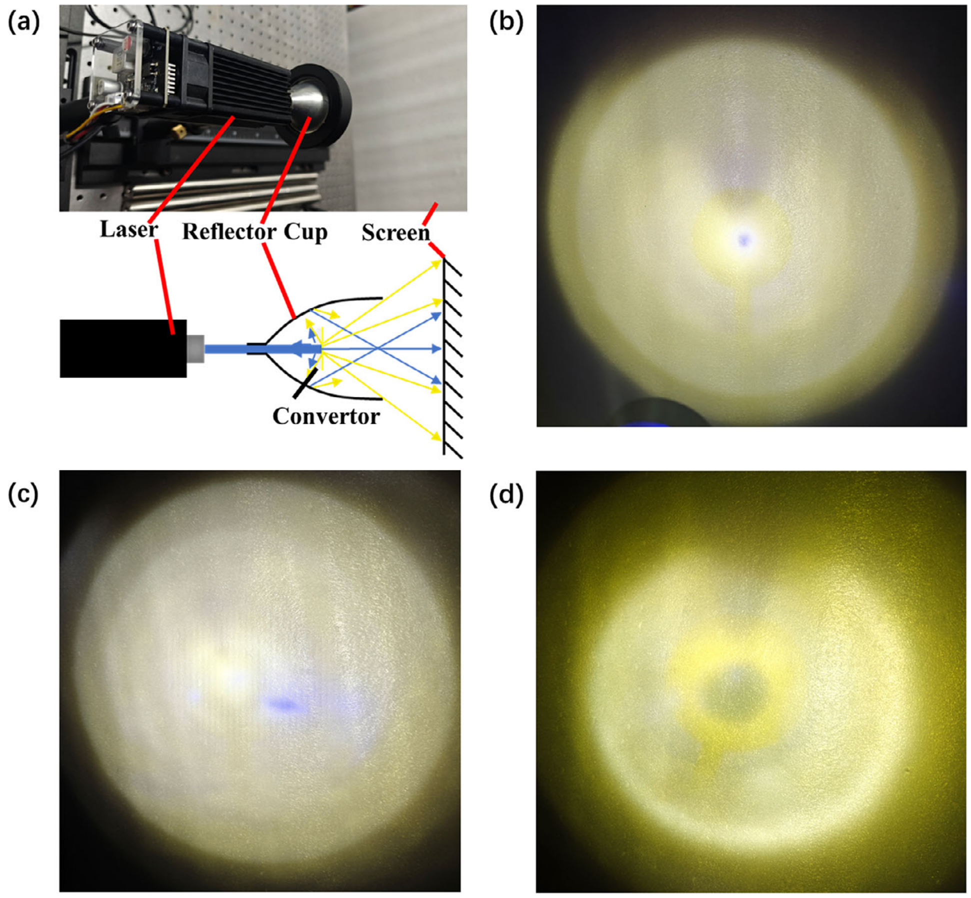

FIGURE 8 | (a) Photograph and schematic diagram of the device for demonstrating the mixed light spot from converter and blue laser. Light spots of (b) PiF-F, (c) PiF-GS-S, and (d) PiF-GS-O projected on the white screen.

The actual luminescence effects of these converters have been studied. As shown in Figure 8a, the converters were successively fixed in a reflective cup and illuminated from the substrate side with a 450 nm laser under a laser power density of 3.48 W/mm^2, projecting the light spot onto a white screen. In the light spot of PiF-F (as shown in Figure 8b), a relatively bright blue laser spot is visible at the center. This is primarily because most of the laser energy is absorbed by the PiF layer, with only a small fraction penetrating the PiF and projecting onto the screen. The light spot of PiF-GS-S (Figure 8c) is similar to that of PiF-F, but due to the reduced transmittance of the patterned substrate, the reflected blue laser light becomes more intense, thereby increasing the CCT of the white light (as shown in Figure 4c). The light spot of PiF-GS-O is presented in Figure 8d. Different from the light spot of PiF-F and PiF-GS-S, the center of PiF-GS-O does not exhibit an obvious blue light spot. Instead, a large area of uniform white light is observed throughout the spot. This also indicates that the laser light incident from the patterned side can be diverged more effectively into a larger region of the PiF.

4 | Conclusions

In this work, sapphire substrate was patterned by ICP etching, and PiFs were prepared on the surface of these substrates using co-sintering method. Microscopic observations revealed that the pattern possessed periodic arrays of convex cross-section grating structure. The YAG:Ce PiF was less affected by high temperature and glass corrosion, and still maintained good luminescent characteristics. Due to the structure, the GS sapphire exhibited strong modulation to the blue laser compared to F, and showed dispersed light spots due to diffraction. With increasing laser power density, PiF-GS-O achieved higher LF (over 1400 lm) and LE (approximately 180 lm/W), as well as a higher saturation power density, which increased by up to 66% compared to PiF-F, reaching 14.48 W/mm^2. By analyzing the pattern's influence on light beams, angular CCT and luminescence effect, we gained deeper insight into the improved luminescence properties of PiF-GS relative to PiF-F. This work provides a novel method to achieve high luminescence performance PiF for laser lighting.

Funding

This work was supported by the Natural Science Foundation of Xiamen, China (3502Z202572005), and the Shenzhen Science and Technology Program (ZDSYS20220527171201003).

Conflicts of Interest

The authors declare no conflicts of interest.

Data Availability Statement

Data underlying the results presented in this paper may be obtained from the authors upon reasonable request.

References

1. J. J. Wierer Jr., J. Y. Tsao, and D. S. Sizov, “Comparison Between Blue Lasers and Light-Emitting Diodes for Future Solid-State Lighting,” *Laser & Photonics Reviews* 7 (2013): 963–993, https://doi.org/10.1002/lpor.201300048.

2. S. Liu, P. Sun, Y. Liu, et al., “Warm White Light With a High Color-Rendering Index From a Single $Gd_3Al_4GaO_{12}$:Ce^{3+} Transparent Ceramic for High-Power LEDs and LDs,” *ACS Applied Materials & Interfaces* 11 (2019): 2130–2139, https://doi.org/10.1021/acsami.8b18103.

3. J.-S. Kim, S. Yang, and B.-S. Bae, “Thermally Stable Transparent Sol−Gel Based Siloxane Hybrid Material With High Refractive Index for Light Emitting Diode (LED) Encapsulation,” *Chemistry of Materials* 22 (2010): 3549–3555, https://doi.org/10.1021/cm100903b.

4. X. Zhang, L. Huang, F. Pan, et al., “Highly Thermally Stable Single-Component White-Emitting Silicate Glass for Organic-Resin-Free White-Light-Emitting Diodes,” *ACS Applied Materials & Interfaces* 6 (2014): 2709–2717, https://doi.org/10.1021/am405228x.

5. E. G. Víllora, S. Arjoca, D. Inomata, and K. Shimamura, “Single-Crystal Phosphors for High-Brightness White LEDs/LDs,” in *Proceedings of SPIE - The International Society for Optical Engineering*, eds. H. Jeon, L.-W. Tu, M. R. Krames, and M. Strassburg (SPIE, 2016), 976805.

6. G. Gu, W. Xiang, C. Yang, and X. Liang, “Synthesis and Luminescence Properties of a H_2 Annealed Mn-Doped $Y_3Al_5O_{12}$:Ce^{3+} Single Crystal for WLEDs,” *CrystEngComm* 17 (2015): 4554–4561, https://doi.org/10.1039/C5CE00641D.

7. Q. Yao, P. Hu, P. Sun, et al., “YAG:Ce^{3+} Transparent Ceramic Phosphors Brighten the Next-Generation Laser-Driven Lighting,” *Advanced Materials* 32 (2020): 1907888, https://doi.org/10.1002/adma.201907888.

8. S. Zhuo, S. Lin, T. Pang, et al., “Transparent Ceramic-Quantum Dots Glass Film Composites With High-Efficiency Thermal Management for Laser-Driven Projection Display,” *Advanced Functional Materials* 36 (2026): e16371, https://doi.org/10.1002/adfm.202516371.

9. D. Hu, S. Lin, T. Pang, et al., “Ultra-Narrowband Green-Emitting Transparent Composite Ceramics for Laser-Driven Display,” *Advanced Materials* 37 (2025): 2414957, https://doi.org/10.1002/adma.202414957.

10. J. Xu, Y. Yang, Z. Guo, et al., “Comparative Study of Al_2O_3-YAG:Ce Composite Ceramic and Single Crystal YAG:Ce Phosphors for High-Power Laser Lighting,” *Ceramics International* 46 (2020): 17923–17928, https://doi.org/10.1016/j.ceramint.2020.04.101.

11. Y. H. Song, E. K. Ji, B. W. Jeong, M. K. Jung, E. Y. Kim, and D. H. Yoon, “High Power Laser-Driven Ceramic Phosphor Plate for Outstanding Efficient White Light Conversion in Application of Automotive Lighting,” *Scientific Reports* 6 (2016): 31206, https://doi.org/10.1038/srep31206.

12. S. Liao, S. Jin, T. Pang, et al., “Novel Color Converters for High Brightness Laser-Driven Projection Display: Transparent Ceramics–Glass Ceramics Film Composite,” *Advanced Functional Materials* 34 (2024): 2307761, https://doi.org/10.1002/adfm.202307761.

13. X. Zhang, J. Yu, J. Wang, et al., “All-Inorganic Light Convertor Based on Phosphor-in-Glass Engineering for Next-Generation Modular High-Brightness White LEDs/LDs,” *ACS Photonics* 4 (2017): 986–995, https://doi.org/10.1021/acsphotonics.7b00049.

14. J. Yu, S. Si, Y. Liu, et al., “High-Power Laser-Driven Phosphor-in-Glass for Excellently High Conversion Efficiency White Light Generation for Special Illumination or Display Backlighting,” *Journal of Materials Chemistry C* 6 (2018): 8212–8218, https://doi.org/10.1039/C8TC01178H.

15. S. Bao, Y. Liang, L. Wang, et al., “Superhigh-Luminance Ce:YAG Phosphor in Glass and Phosphor-in-Glass Film for Laser Lighting,” *ACS Sustainable Chemistry & Engineering* 10 (2022): 8105–8114, https://doi.org/10.1021/acssuschemeng.2c02657.

16. H. Wang, Y. Mou, Y. Peng, et al., “Fabrication of Phosphor Glass Film on Aluminum Plate by Using Lead-Free Tellurite Glass for Laser-Driven White Lighting,” *Journal of Alloys and Compounds* 814 (2020): 152321, https://doi.org/10.1016/j.jallcom.2019.152321.

17. H. Zhang, J. Zhao, Z. Yu, et al., “A Novel Sapphire@PiGF@Sapphire Color Converter With High Luminescence Saturation Threshold for Laser Lighting,” *Advanced Functional Materials* 35 (2025): 2414023, https://doi.org/10.1002/adfm.202414023.

18. P. Zheng, S. Li, L. Wang, et al., “Unique Color Converter Architecture Enabling Phosphor-in-Glass (PiG) Films Suitable for High-Power and High-Luminance Laser-Driven White Lighting,” *ACS Applied Materials & Interfaces* 10 (2018): 14930–14940, https://doi.org/10.1021/acsami.8b03168.

19. R. Wei, L. Wang, P. Zheng, et al., “On the Luminance Saturation of Phosphor-in-Glass (PiG) Films for Blue-Laser-Driven White Lighting: Effects of the Phosphor Content and the Film Thickness,” *Journal of the European Ceramic Society* 39 (2019): 1909–1917, https://doi.org/10.1016/j.jeurceramsoc.2019.01.024.

20. J. Xu, B. Liu, Z. Liu, et al., “Design of Laser-Driven SiO_2-YAG:Ce Composite Thick Film: Facile Synthesis, Robust Thermal Performance, and Application in Solid-State Laser Lighting,” *Optical Materials* 75 (2018): 508–512, https://doi.org/10.1016/j.optmat.2017.10.049.

21. D.-H. Lee, S. Kim, H. Kim, and S.-K. Lee, “Highly Efficient and Highly Conductive Phosphor-in-Glass Materials for Use in LD-Driven White-Light Lamp,” *International Journal of Precision Engineering and Manufacturing-Green Technology* 6 (2019): 293–303, https://doi.org/10.1007/s40684-019-00054-z.

22. Z. Yu, J. Zhao, Z. Yang, et al., “A Novel PiGF@Diamond Color Converter With a Record Thermal Conductivity for Laser-Driven Projection Display,” *Advanced Materials* 36 (2024): 2406147, https://doi.org/10.1002/adma.202406147.

23. S. Lin, H. Lin, Q. Huang, et al., “Highly Crystalline $Y_3Al_5O_{12}$:Ce^{3+} Phosphor-in-Glass Film: A New Composite Color Converter for Next-Generation High-Brightness Laser-Driven Lightings,” *Laser & Photonics Reviews* 16 (2022): 2200523, https://doi.org/10.1002/lpor.202200523.

24. H. Wu, Z. Hao, G.-H. Pan, et al., “Phosphor-SiO_2 Composite Films Suitable for White Laser Lighting With Excellent Color Rendering,” *Journal of the European Ceramic Society* 40 (2020): 2439–2444, https://doi.org/10.1016/j.jeurceramsoc.2020.01.020.

25. J. Zhao, Y. Mou, Z. Yu, et al., “Microstructured Interface Modification of Laser-Driven Phosphor-in-Glass-Film for Ultra-High-Efficiency White Lighting,” *Journal of Alloys and Compounds* 960 (2023): 170744, https://doi.org/10.1016/j.jallcom.2023.170744.

26. W. Ding, S. Yang, X. Hou, et al., “High Performance Composite Phosphor-in-Glass Film for Laser-Driven Warm White Light on Patterned Sapphire Substrate,” *Journal of Materiomics* 11 (2025): 100892, https://doi.org/10.1016/j.jmat.2024.04.014.

27. S. Zhou and S. Liu, “Study on Sapphire Removal for Thin-Film LEDs Fabrication Using CMP and Dry Etching,” *Applied Surface Science* 255 (2009): 9469–9473, https://doi.org/10.1016/j.apsusc.2009.07.063.

28. Y. P. Hsu, S. J. Chang, Y. K. Su, et al., “ICP Etching of Sapphire Substrates,” *Optical Materials* 27 (2005): 1171–1174, https://doi.org/10.1016/j.optmat.2004.08.076.

29. T. Zhong, G. Guo, Y. Chow, et al., “Measurement Method of Refractive Index for Optical Lenses Based on Curvature Radius Fitting of Small-Sized Aspheric Surfaces,” *Optics* 6 (2025): 4, https://doi.org/10.3390/opt6010004.